Ersch. in: Research methods in biomineralization science / James J. De Yoreo (ed.). - Amsterdam [u.a.] : Elsevier, Acad. Press, 2013. - S. 45-69. - (Methods in enzymology ; 532). - ISBN 978-0-12-416617-2

http://dx.doi.org/10.1016/B978-0-12-416617-2.00003-5

Investigating the Early Stages of Mineral Precipitation by Potentiometric Titration and Analytical Ultracentrifugation

Matthias Kellermeier, Helmut Cölfen, Denis Gebauer[1]

Department of Chemistry, Physical Chemistry, University of Konstanz, Konstanz, Germany
[1]Corresponding author: e-mail address: denis.gebauer@uni-konstanz.de

Contents

Abstract

Despite the importance of crystallization for various areas of research, our understanding of the early stages of the mineral precipitation from solution and of the actual mechanism of nucleation is still rather limited. Indeed, detailed insights into the processes underlying nucleation may enable a systematic development of novel strategies for controlling mineralization, which is highly relevant for fields ranging from materials chemistry to medicine. In this work, we describe experimental aspects of a quantitative assay, which relies on pH titrations combined with *in situ* metal ion potentiometry and conductivity measurements. The assay has originally been designed to study the crystallization of calcium carbonate, one of the most abundant biominerals. However, the developed procedures can also be readily applied to any compound containing cations for which ion-selective electrodes are available. Besides the possibility to quantitatively

assess ion association prior to nucleation and to directly determine thermodynamic solubility products of precipitated phases, the main advantage of the crystallization assay is the unambiguous identification of the different stages of precipitation (i.e., prenucleation, nucleation, and early postnucleation) and the characterization of the multiple effects of additives. Furthermore, the experiments permit targeted access to distinct precursor species and intermediate stages, which thus can be analyzed by additional methods such as cryo-electron microscopy or analytical ultracentrifugation (AUC). Regarding ion association in solution, AUC detects entities significantly larger than simple ion pairs, so-called prenucleation clusters. Sedimentation coefficient values and distributions obtained for the calcium carbonate system are discussed in light of recent insights into the structural nature of prenucleation clusters.

1. INTRODUCTION

Crystallization phenomena are ubiquitous in daily life and bear fundamental importance for a broad variety of scientific disciplines, ranging from materials chemistry and crystallography over pharmacy and medicine to industrial processing. Still, much effort is devoted to study biomineralization processes (Lowenstam & Weiner, 1989), as the obtained insight may be utilized in bio inspired approaches to novel functional materials with potential applications in diverse fields (Fratzl & Weiner, 2010; Sommerdijk & Cölfen, 2010; Weiner & Addadi, 2011). In recent years, there is increasing evidence that the classical textbook perspective (Mullin, 2001) on nucleation and growth of minerals fails to explain a number of crystallization phenomena and thus seems to have rather limited relevance, at least in some systems (Banfield, Welch, Zhang, Ebert, & Penn, 2000; Cölfen & Antonietti, 2008; Gebauer & Cölfen, 2011; Li et al., 2012; Meldrum & Cölfen, 2008). It is now widely accepted that mineralization sequences according to Ostwald's rule of stages is a common phenomena; that is, the initially precipitated phase is not necessarily the most stable polymorph under the given conditions and, in particular, that amorphous precipitates are common precursors in the crystallization of a number of minerals (Weiner, Mahamid, Politi, Ma, & Addadi, 2009). In fact, such intermediates appear to play a key role in the directed self assembly of crystalline structures with complex morphologies, both in biological and bio inspired environments (Addadi, Raz, & Weiner, 2003; Gower, 2008). Regarding the onset of precipitation, classical theories assume that the first nuclei in solution are formed via stochastic collisions of atoms, ions, or molecules (depending on the type of crystal). Eventually, this leads to the occurrence of a metastable

cluster—the critical nucleus—which subsequently grows to a macroscopic crystal via continuous addition of these monomers (De Yoreo & Vekilov, 2003). As opposed to that, so called nonclassical concepts have been reported, where the species considered to be central to mineral nucleation and growth are significantly larger than the basic atomic or molecular con stituents and may range from stable solute clusters to nanoparticle building units (Cölfen & Antonietti, 2008; Gebauer & Cölfen, 2011).

For the study of nucleation phenomena, induction time statistics have often been employed (Izmailov, Myerson, & Arnold, 1999); however, in most cases, this approach cannot shed light on the fundamental processes that underlie nucleation by principle (Davey, Schroeder, & ter Horst, 2013). As pointed out by the latter authors, it is crucial to investigate solute association in order to obtain a novel—molecular—perspective on nucleation. In the 1970s, it was recognized that any change in intensive parameters such as pH can sensibly affect nucleation and growth; therefore, the constant composition method was established so as to allow for truly quantitative physicochemical analyses (Tomson & Nancollas, 1978). Inspired by this technique, we have designed a crystallization assay in which supersaturation is slowly generated under otherwise constant (or explicitly known and con trolled) conditions, while the concentrations of relevant species are contin uously monitored. Corresponding measurements have led to the discovery and characterization of so called prenucleation clusters in solutions of cal cium carbonate (Gebauer, Völkel, & Cölfen, 2008) and moreover have shown that amorphous intermediates with distinct short range structures are generated at different pH levels in the absence of any additives (Gebauer et al., 2010, 2008). By using the developed methodology, it is pos sible to quantitatively assess ion association in solution, to trace the nucle ation event and its kinetics, and to examine the nature of initially formed nanoparticles of amorphous calcium carbonate (ACC) and their subsequent transformation toward more stable (crystalline) polymorphs. Beyond that, the role and effect of certain additives during the distinct stages of precipi tation can be evaluated (Gebauer, Cölfen, Verch, & Antonietti, 2009) and, for instance, used to optimize industrial products like scale inhibitors. With respect to fundamental analyses of early precursor phases, the crystallization assay offers the advantage that it clearly indicates, at all times, the stage in which a given sample currently exists (i.e., still prenucleation, near or at nucleation, or already postnucleation). This sets a valuable basis for in depth studies of these distinct stages, for example, by means of cryo electron microscopy (Dey, de With, & Sommerdijk, 2010) or analytical

ultracentrifugation (AUC) (Planken & Cölfen, 2010), which have turned out to be especially powerful techniques in this context.

Herein, we detail the basic equipment for this crystallization assay, give an outline of experimental procedures and evaluation routines, and finally exemplify how AUC can be used to investigate solute association prior to nucleation. Recent advancements and crucial points in data analysis and interpretation are critically discussed. We hope that this contribution will foster further research into the role of ion association during the early stages of crystallization, which may lead to a better understanding of nucleation mechanisms in general. In the following, we will focus on experiments con ducted with calcium carbonate as a model system but note that the presented methodology can be directly transferred to other calcium minerals like phos phates, oxalates, or sulfates as well. Furthermore, with suitable ion selective electrodes (commercial or self made), a vast amount of other materials is analytically accessible in an analogous manner.

2. EQUIPMENT

2.1. Titration setup

Our measurements are performed using a computer controlled titration sys tem supplied by Metrohm (Filderstadt, Germany), with corresponding commercial software (Tiamo™, current version: 2.3). The principal setup consists of a titration instrument (Titrando 905, Metrohm No. 2.905.0020) that controls two dosing devices (Dosino 800, Metrohm No. 2.800.0010), which in turn operate two 807 Dosing Units (Metrohm No. 6.3032.120, one each for addition of $CaCl_2$ and NaOH solution; see succeeding text). The whole assembly is run by an independent power sup ply, which decouples the electric circuit of the instruments from that of the laboratory. The dosing units are equipped with 2 mL glass cylinders as inter nal reservoirs, which allow titrant solutions to be dispensed in volume steps down to 200 nL, thereby rendering very fine and precise titrations possible. Different pH electrodes are employed depending on actual needs and requirements, such as fast response times (Metrohm Flat Membrane Elec trode, No. 6.0256.100), robustness at elevated temperatures (Metrohm Unitrode, No. 6.0258.010), small sample volumes (Metrohm Biotrode, No. 6.0224.100), or routine applications (Metrohm Microelectrode, No. 6.0234.100). In order to measure free concentrations of Ca^{2+} during titration, we use calcium ion selective electrodes (Ca^{2+} ISE, Metrohm No. 6.0508.110 (half cell) or 6.0510.100 (combined sensor)) and, if

required, tap the potential of the internal Ag/AgCl reference system of the pH electrode.

The setup can be extended to also monitor the conductivity of the studied solutions by a conductometric cell (Metrohm No. 6.0910.120 or 6.0915.130) connected via a corresponding module (Conductivity Module 856, Metrohm No. 2.856.0010), while the turbidity of the samples can be traced by means of an appropriate optical sensor (Optrode, Metrohm No. 6.1115.000; this option will however not be discussed further hereinafter). For quantitative analyses, experiments are carried out in commercial double walled titration vessels (Metrohm Nos. 6.1418.220 and 6.1414.010), which are fed by oil from an attached thermostat, so that the temperature of the receiver solution (measured by an immersed Pt100 probe) is maintained at a preset value in the range of 10–90 °C (usually 25 °C). The vessels are closed and largely decoupled from the atmosphere, in order to minimize potential artifacts that may arise from in diffusion of atmospheric CO_2 or evaporation of the solutions, especially at higher temperatures.

2.2. Analytical ultracentrifuge

We use a Beckman Coulter XL I ultracentrifuge equipped with Rayleigh interference optics for detecting sedimenting species via spatiotemporal changes in refractive index. Measurements are performed at 25 °C and a rotor speed of 60,000 RPM in self made 12 mm 2.5° titanium double sector centerpieces, with at least 8 h duration per experiment. Resulting primary data are processed and evaluated using the SEDFIT program, in which $c(s)$ as well as Lamm equation modeling is performed (Schuck, 2000, 2013).

3. EXPERIMENTAL PROCEDURES

3.1. Calibration of electrodes and sensors

3.1.1 Ca^{2+}-ISE

When sparingly soluble minerals like calcium carbonate are investigated, calibration of the Ca^{2+} ISE can be conducted in water, because ionic strengths in the actual measurements are rather low ($\leq$20 m*M*) and can be neglected to a good approximation. Indeed, very recent work has quantitatively confirmed earlier qualitative claims (Gebauer & Cölfen, 2011) that contributions originating from ionic activity just slightly exceed the range of typical experimental error and that ideal treatment does not affect as determined physicochemical parameters (binding constants and free energies, and solubility products) to any significant extent (Kellermeier,

Picker, Kempter, Cölfen, & Gebauer, 2013). Thus, for calibration, 10 m*M* calcium chloride solution is dosed at a constant rate of 10 μL/min into 50 mL water (Milli Q quality), which has been adjusted to the pH of the subsequent crystallization experiment by adding aliquots of 10 m*M* NaOH. During titration, the receiver solution is continuously stirred and showered with a gentle stream of water saturated nitrogen to avoid CO_2 in diffusion. Simultaneously, any decrease in pH due to addition of the slightly acidic Ca^{2+} solution is automatically counterbalanced by titration with 10 m*M* NaOH. The Ca^{2+} potential is recorded every 10 s and, since all added vol umes are known at any time, can be related to the actual calcium concen tration via a Nernstian approach according to

$$U\left(Ca^{2+}\right) = U_0 + \frac{RT}{2F}\ln\left[c\left(Ca^{2+}\right)\right] \tag{3.1}$$

where $U(Ca^{2+})$ is the measured potential, U_0 the electrode intercept, R the gas constant, T the temperature, and F the Faraday constant. In principle, calibration is carried out mainly to determine the electrode intercept U_0, since the slope is given as $m = RT/2F$ in case of Nernstian behavior. How ever, for data analysis, we always use the values obtained from calibration, in order to account for any possible deviations. Then, the potentials measured in the subsequent crystallization assays can be converted into concentrations by using Eq. (3.1) and the as obtained values for U_0 and m, under the assumption of ideality (Kellermeier et al., 2013). We normally calibrate Ca^{2+} selective electrodes at least once per week.

On the other hand, when the analyzed solutions exhibit noticeably higher ionic strengths ($I > \sim 25$ m*M*)—for example, due to the presence of charged additives or when more soluble minerals are investigated—the error made by ideal treatment (and calibration in water) becomes significant, and the ISE should preferably be calibrated in ionic strength adjusted envi ronments. This can be realized by titrating $CaCl_2$ into solutions containing suitable amounts of sodium chloride as a background electrolyte, meant to emulate the ionic strength in the samples. In this way, activity effects that arise from Coulomb interactions are accounted for in calibration (they affect primarily the electrode intercept U_0), and resulting U_0^{NaCl} and m values allow for directly translating experimental potentials into actual free Ca^{2+} concen trations (Kellermeier et al., 2013). In turn, when accurate thermodynamic parameters are to be derived from the titration data, these concentrations have to be converted into activities. The required activity coefficients can be either directly obtained from a comparison of ISE calibrations in water

and NaCl solutions (Kellermeier et al., 2013) or calculated with the aid of theoretical expressions that are suitable for the given range of ionic strengths (such as extended Debye–Hückel or Davies equations) (Robinson & Stokes, 2002).

3.1.2 pH electrodes

Calibration of the pH electrodes is achieved by means of a three point routine utilizing commercial buffers from Mettler Toledo (pH 4.00, 7.00, and 9.21). Biweekly calibration has turned out to be sufficient.

3.1.3 Conductivity probes

For accurate conductivity measurements, the cell constant of the employed probe needs to be determined precisely. In general, the transport of electricity in salt solutions is characterized by Ohm's electrical resistance (R_Ω), which can be expressed as the product of the (shape independent) specific resistance ρ (in Ωm) and the cell constant Z (in m^{-1}), which accounts for the particular geometry of the experimental setup. Specific conductivity (χ, in S/m) and resistance are directly related by $\chi = 1/\rho$. In order to determine the cell constant, R_Ω is measured in a fixed geometrical setting (as defined by the construction of the sensor) for an electrolyte with known conductivity. For the latter purpose, we use potassium chloride standard solutions supplied by Merck (CertiPUR, either 0.01 *M* (1.41 mS/cm) or 0.1 *M* (12.88 mS/cm), depending on the estimated range of χ in the samples). In this way, measured resistance values can be converted into normalized specific conductivities, which then may be used to calculate ion concentrations in an alternative approach.

3.2. Crystallization assay: Potentiometry, conductivity, and pH titration

A schematic illustration of the experimental setup is shown in Fig. 3.1A. In the crystallization assays, 10 m*M* calcium chloride solution is titrated at a rate of 10 μL/min into 50 mL 10 m*M* sodium (bi)carbonate buffer at a given preset pH, applying the same routine as detailed earlier for the ISE calibration. Calcium potentials, pH, and conductivity values are read from the immersed probes in intervals between 2 and 10 s. Carbonate buffers can be readily prepared by mixing appropriate volumes of 10 m*M* $NaHCO_3$ and 10 m*M* Na_2CO_3, until the desired pH is reached (the overall carbonate concentration thus remains 10 m*M*). The fraction of CO_3^{2-} ions is very low (<0.05%) at neutral pH values and increases from ca. 4% to 25% as the pH is raised from 9 to 10. Therefore, association of Ca^{2+} and CO_3^{2-} in solution

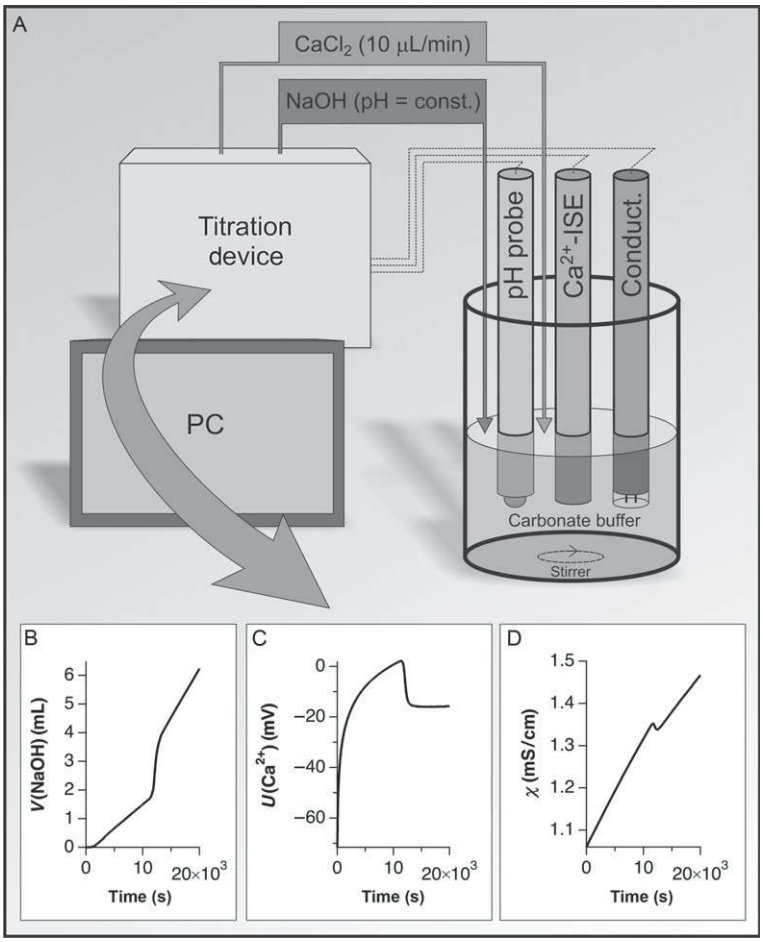

Figure 3.1 Schematic overview of the employed titration setup (A) with plots showing the time developments of typical primary data (B–D, raw data). The titration device is controlled by a computer (PC) and operates two dosing units for the continuous addition of calcium chloride and sodium hydroxide solution (the latter being used for keeping the pH constant by automatic countertitration). Three sensors are connected: a pH probe, a calcium ion-selective electrode (Ca^{2+}-ISE), and a conductivity sensor (Conduct.). During addition of $CaCl_2$, the volume of NaOH necessary to maintain the preset pH value (V(NaOH) in B), the calcium potential ($U(Ca^{2+})$ in C), and the specific conductivity (χ in D) are recorded. Upon nucleation of $CaCO_3$, all curves respond by a distinct change.

prior to nucleation has been examined in the latter range (Gebauer et al., 2008), while experiments at near neutral pH have evidenced that binding of HCO_3^- to Ca^{2+} occurs only upon nucleation of a liquid intermediate (and *not* significantly before nucleation) (Bewernitz, Gebauer, Long, Cölfen, & Gower, 2012).

In the course of $CaCl_2$ addition, the pH of the (bi)carbonate solution has to be kept constant by countertitration of 10 m*M* NaOH, as in the case of the calibrations. However, this effect is much more pronounced in the buffer, because binding of carbonate ions in $CaCO_3$ species (before, during, and after nucleation) leads to the effective removal of a base or, in other words, to a decrease in pH. The volume of sodium hydroxide required to maintain a constant pH level can be used to calculate the absolute amount of carbonate bound at any given stage (Gebauer et al., 2008), as detailed later. We note that NaOH solutions are not titer stable and hence should be pre pared freshly for quantitative analyses. As already indicated earlier, this pH titration is performed automatically by the computer controlled system. A fundamental prerequisite for accurate pH titrations is that the electrode potential has stabilized before Ca^{2+} addition is started (which typically takes about 1–2 min), so as to avoid overtitrations. Moreover, the set point of the titration needs to be precisely adjusted to the actual pH value of the buffer. Although pH measurements generally have an absolute error in the range of 0.05 units, our setup displays three digits in order to facilitate fine tuning. Typically, the measured pH of the buffer agrees with the preset value within 0.01–0.03 units. The set point for the titration is then adjusted to ca. 0.005 pH units below the measured current value of the buffer, before ini tiating the addition of $CaCl_2$. Apart from the set point itself, the success of the automatic countertitrations relies on three further parameters (in Tiamo), namely, the dynamic pH range, the minimum addition rate, and maximum addition rate. For our particular setting, optimal results are obtained for a dynamic range of 0.1 pH units, a minimum rate of 5 μL/min, and a maximum rate of 2 mL/min.

3.3. Sample preparation for AUC measurements

In order to analyze solute association by means of AUC, aliquots are drawn from the crystallization assay at distinct stages prior to nucleation. The nucle ation process is concurrently indicated by a steep increase in the volume of NaOH needed to maintain the pH (Fig. 3.1B), a drop in the amount of free Ca^{2+} detected by the ISE (Fig. 3.1C), as well as a kink in the development of the measured conductivity (Fig. 3.1D). Hence, it is possible to directly assess which state is actually analyzed, that is, at which level of under or super saturation the samples were in fact drawn. Aliquots of the solutions are immediately filled into the AUC cells and subsequently analyzed in so called sedimentation velocity experiments (Demeler, 2005), which yield—as a primary result—the sedimentation coefficient (*s*) distribution

for a predefined number of distinct components (see succeeding text). However, also, Diffusion coefficients (D) are also accessible from the data by analyzing the time dependent broadening of sedimenting boundaries. Detailed experimental procedures—concerning, for example, the appropriate filling of cells, calibrations of radial position and angular velocity, or balancing of the rotor—are described in the literature (Mächtle & Börger, 2006; Ralston, 1993).

4. DATA EVALUATION

4.1. Treatment of primary data from the titration setup

First, it is important to note that ion selective electrodes only detect single and free—that is, noncomplexed and unbound—ions in their hydrated state. Thus, the recorded Ca^{2+} potential (Fig. 3.1C) reflects the concentration (when ideality is assumed; otherwise, it reflects the activity) of free calcium ions, $c_{free}(Ca^{2+})$, which is accessible via Eq. (3.1). In turn, since the dosed amount of calcium, that is, the total concentration of Ca^{2+} present in the system $c_{added}(Ca^{2+})$, is known at all times, the concentration of bound calcium, $c_{bound}(Ca^{2+})$, can readily be calculated according to

$$c_{bound}\left(Ca^{2+}\right) = c_{added}\left(Ca^{2+}\right) \quad c_{free}\left(Ca^{2+}\right) \tag{3.2}$$

Second, the volume of NaOH needed to keep the pH constant (Fig. 3.1B) correlates with the amount of base removed from the buffer. With the known buffer composition at the given pH (i.e., the fractions of HCO_3^- and CO_3^{2-} in equilibrium), the amount of added NaOH can be directly converted into absolute numbers of bound carbonate ions (Gebauer et al., 2008). This treatment neglects association between calcium and bicarbonate ions, which, however, is a good approximation at pH levels above ca. pH 8.5 (Kellermeier et al., 2013). Countertitration with NaOH accounts for the removal of diprotic base (CO_3^{2-}) as well as for protons generated by dissociation of bicarbonate ions ($HCO_3^- \rightarrow CO_3^{2-} + H^+$) as the equilibrium carbonate/bicarbonate ratio at the given pH is restored. On that basis, the amount of bound carbonate, $n_{bound}(CO_3^{2-})$, can be calculated from the titrated volume of sodium hydroxide solution, V(NaOH), with its concentration, c(NaOH), and the pH dependent fractions of carbonate, $\lambda(CO_3^{2-})_{pH}$, and bicarbonate ions, $\lambda(HCO_3^-)_{pH}$, in the buffer by the following equation (Gebauer et al., 2008):

$$m_{\text{bound}}\left(CO_3^{2-}\right) = c(\text{NaOH}) \cdot V(\text{NaOH}) \cdot \left[2 \cdot \lambda\left(CO_3^{2-}\right)_{\text{pH}} + \lambda(HCO_3^-)_{\text{pH}}\right]^{-1} \tag{3.3}$$

For calcium carbonate, such analyses evidence that equal amounts of CO_3^{2-} and Ca^{2+} ions are bound throughout the different stages within experimental accuracy and, hence, that any associated prenucleation species are neutral in charge on average (Gebauer et al., 2008). Similar expressions can be derived for the binding of phosphate species during calcium phosphate precipitation. In turn, for (very) weak bases like sulfate or oxalate, there will be only minor effects on pH upon ion association, and anion binding cannot be quantified via pH titration for corresponding minerals.

Third, the measured conductivity values (Fig. 3.1D) result from the contributions of all cations and anions in the system, which can be modeled using Kohlrausch's law of independent ion migration for the case of infinite dilution (ideal conditions) or a combination of Fuoss–Onsager equations for nonideal behavior at higher ionic strengths (Robinson & Stokes, 2002). Hence, concentrations of free and bound Ca^{2+} and CO_3^{2-} ions can be calculated from the conductivity data and applied to test values obtained from calcium potential measurements and pH titrations. On the one hand, this allows for confirming the validity of certain assumptions made, for example, that calcium bicarbonate association can be neglected at the investigated pH levels. On the other hand, when combined with ISE data, the conductivity measurements provide an alternative means to assess anion binding in situations where pH titrations do not give corresponding information (i.e., for weakly basic anions).

Practically, we use spreadsheet analyses to process primary data sets, which are imported as tables together with calibration values as well as initial concentrations and volumes, in order to derive relevant secondary quantities (such as bound amounts of Ca^{2+} and CO_3^{2-}) at any time during the titration. Commonly, each experiment is performed at least in triplicate, so as to ensure reproducibility and estimate experimental errors simultaneously. Figure 3.2 shows a scheme depicting the typical development of detected free Ca^{2+} during the early stages of $CaCO_3$ precipitation (dashed line), as obtained by evaluation of the primary data displayed in Fig. 3.1C. Initially, the measured amount of free calcium increases linearly until a maximum is reached, which corresponds to a critical stage where phase separation occurs. At this point, solid particles are nucleated and the calcium level rapidly drops to a plateau that reflects the solubility of

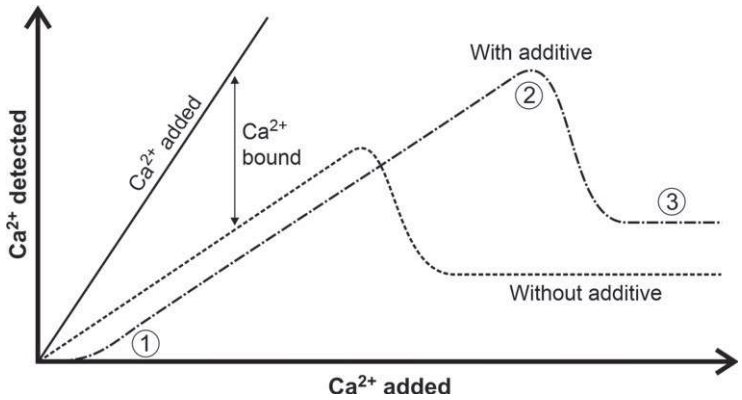

Figure 3.2 Qualitative representation of the amount of Ca^{2+} detected during titration of $CaCl_2$ into dilute carbonate buffer in the absence (dashed line) and presence (dashed dotted line) of an additive. In both cases, significantly less Ca^{2+} is measured than actually added, reflecting the fraction of calcium bound in each of the different stages. The amount of free Ca^{2+} first increases linearly and then drops to a level corresponding to the solubility of the phase formed upon nucleation. From changes in distinct features of the curve, the influence of crystallization additives can be directly identified and characterized. The hypothetical additive depicted in the plot shows the following effects: (1) complexation of calcium ions, (2) inhibition of nucleation, and (3) stabilization of a more soluble phase after nucleation.

the precipitated phase (usually amorphous $CaCO_3$ under the given conditions). In the presence of additives, the different features of the curves can change markedly, allowing the various possible roles of crystallization additives to be quantified and categorized (Gebauer, Cölfen, et al., 2009; Verch, Gebauer, Antonietti, & Cölfen, 2011). Figure 3.2 (dashed dotted line) exemplifies a case where an additive is able to (i) complex Ca^{2+} ions (apparent from a delayed increase in free calcium), (ii) inhibit nucleation (causing a shift of maximum in the curve toward larger amounts of added calcium and, thus, higher supersaturation), and (iii) induce the formation of a less stable solid phase (reflected by an increase in solubility). Indeed, other effects like destabilization of ion associates in the prenucleation regime or growth inhibition of precipitated particles can also be quantitatively characterized by such titrations (both not being explicitly shown in Fig. 3.2).

Finally, the data enable direct calculation of actual free ion products ($IP = c_{free}(Ca^{2+}) \cdot c_{free}(CO_3{}^{2-})$) during any of the distinct stages of precipitation probed by the experiments. In principle, corresponding values result immediately from thorough analyses of primary data, as the calcium concentration is measured by the ion selective electrode, while the carbonate

concentration can be independently obtained from the pH titration and/or conductivity data. However, since 1:1 binding of the ions has been demonstrated for the $CaCO_3$ system (cf. preceding text), it is practically sufficient to measure free concentrations of Ca^{2+} with an ISE and derive those of CO_3^{2-} via straightforward mass balance considerations; that is, subtract the number of bound calcium from the total amount of carbonate present and restore the bicarbonate/carbonate equilibrium under the new conditions according to

$$c_{\text{free}}\left(CO_3^{2-}\right) = \lambda\left(CO_3^{2-}\right)_{\text{pH}} \cdot \left[n_{\text{total}}\left(HCO_3^{-}/CO_3^{2-}\right) - n_{\text{bound}}\left(Ca^{2+}\right)\right] \cdot V_{\text{total}}^{-1} \tag{3.4}$$

In this way, the titrations readily give access to thermodynamic solubility products of solid phases detected after nucleation (Kellermeier et al., 2013) and thus allow for the identification and characterization of any occurring metastable intermediates, both in the absence (Gebauer et al., 2010) and presence of additives (Gebauer, Cölfen, et al., 2009; Gebauer, Verch, Börner, & Cölfen, 2009; Picker, Kellermeier, Seto, Gebauer, & Cölfen, 2012; Verch et al., 2011).

4.2. Advanced analyses: The multiple-binding equilibrium

The temporal profiles traced for the concentrations of the relevant ions using titration as well as potentiometric and conductometric experimentation can further be used to derive thermodynamic parameters for ion associates existing in solution prior to nucleation, based on different models. First of all, it is crucial to emphasize that any successful description of experimental results by a certain assumed model cannot prove the validity of this model as such, because any theory always poses distinct basic axioms. A given physicochemical model that fits actual data should be critically assessed whether it bears the ability to make predictions while admitting that there might always be other models with greater explanatory power. On the other hand, if the chosen model is incompatible with experimental observations, the only safe conclusion to be drawn is that it relies on insufficient (not necessarily erroneous) assumptions.

In the case of calcium carbonate, association in solution has traditionally been discussed in the framework of ion pairing (i.e., $Ca^{2+}_{(aq)} + CO_3^{2-}{}_{(aq)} \rightarrow [CaCO_3]^0_{(aq)}$), although this concept is still under debate, perhaps owing to the rather large variance in reported equilibrium constants (Gal, Bollinger, Tolosa, & Gache, 1996). One argument being put forward to support the formation of simple ion pairs (rather than

larger associated species) relies on the finding that calcium binding profiles show linear behavior prior to nucleation (cf. Fig. 3.2), as outlined, for instance, by Moore and Verine (1981). Thereby, the thermodynamic equi librium underlying association between n calcium and n carbonate ions is formulated as

$$n\mathrm{Ca}^{2+} + n\mathrm{CO_3}^{2} \rightleftharpoons [\mathrm{CaCO_3}]_n \tag{3.5}$$

If there is a large excess of carbonate species present in the system, changes in the concentration of $\mathrm{CO_3}^{2}$ may be neglected during titration (which, in a rough approximation, is true for our experiments), and the asso ciation constant (K_A) linked to the equilibrium in Eq. (3.5) can be written as follows:

$$\frac{c\left([\mathrm{CaCO_3}]_n\right)}{c^n_{\mathrm{free}}(\mathrm{Ca}^{2+})} = K_A \cdot c^n_{\mathrm{free}}\left(\mathrm{CO_3}^{2}\right) \approx \text{constant} \tag{3.6}$$

Linear binding profiles at constant $\mathrm{CaCl_2}$ addition rates imply that the ratio of free and bound calcium (the latter being equal to n times the concentration of $[\mathrm{CaCO_3}]_n$) remains constant throughout the experiment (or, respectively, during the entire prenucleation stage). With regard to Eq. (3.6), this is obvi ously only possible if $n = 1$ (i.e., ion pair formation). Although this speciation model can successfully describe measured data for $n = 1$, it does not allow to infer that ion pairing is the only explanation for the observed binding behav ior, because any conclusion drawn on the basis of an applied model is strictly confined to the underlying assumptions—such as, in this case, to represent cluster formation as an elementary reaction between a number of constituent ions in a single step according to Eq. (3.5).

In an alternative approach, we may consider the existence of larger ion associates that assemble (and disintegrate) via multiple steps and a series of coupled binding equilibria. The resulting (much more complex) system of equations can be significantly simplified by assuming that all binding events on the way to larger ion associates are independent and equal (Gebauer et al., 2008). At first sight, this may seem to be a drastic simplifi cation, which, however, is sustained by results of extensive computer sim ulations (Demichelis, Raiteri, Gale, Quigley, & Gebauer, 2011; Raiteri & Gale, 2010). Under this particular assumption, binding of ions in ion pairs and higher associates cannot be distinguished anymore from a macroscopic point of view, as the equilibrium described by Eq. (3.5) then has to be reformulated according to

$$Ca^{2+} + CO_3{}^{2} \rightleftharpoons [CaCO_3]_{Cluster} \tag{3.7}$$

where $[CaCO_3]_{Cluster}$ represents an ion pair within a cluster. It is directly evident that, if the chosen model applies, the formation of clusters containing more than one $CaCO_3$ formula unit (actually any arbitrary number) can also be reconciled with linear calcium binding profiles—the expression obtained by this model for the association constant via the law of mass action is mathematically the same as that for the ion pair model discussed earlier.

In order to assess the thermodynamics of cluster formation, we use a so called multiple binding model (Demichelis et al., 2011; Gebauer et al., 2008) that was first introduced for the quantitative analysis of protein–ligand interactions (Scatchard, 1949). It relies on the basic assumption mentioned earlier (equal and independent binding events with identical equilibrium constants K) and formally considers the existence of several binding sites for calcium ions on one carbonate ion, as illustrated by the following reaction scheme:

$$CO_3{}^{2} \underset{K}{\overset{+Ca^{2+}}{\rightleftharpoons}} CaCO_3 \underset{K}{\overset{+Ca^{2+}}{\rightleftharpoons}} [Ca_2CO_3]^{2+} \underset{K}{\overset{+Ca^{2+}}{\rightleftharpoons}} \cdots \tag{3.8}$$

It has to be emphasized that multiple coordination of Ca^{2+} around a central $CO_3{}^{2}$ in a microscopic perspective does not contradict the macroscopically observed 1:1 binding of both ions in prenucleation associates, because the number of binding sites for calcium on carbonate ions, x, does not reflect the stoichiometry of the clusters (Gebauer et al., 2008) and coordination of carbonate on calcium is not necessarily limited to one $CO_3{}^{2}$ per Ca^{2+}, either. Based on the binding scheme indicated by Eq. (3.8), it can be shown that

$$\frac{n_{bound}(Ca^{2+})}{n_{bound}(CO_3{}^{2}) + n_{free}(CO_3{}^{2})} = x \cdot \frac{K \cdot c_{free}(Ca^{2+})}{1 + K \cdot c_{free}(Ca^{2+})} \tag{3.9}$$

where the unknown microscopic parameters x and K are expressed by a combination of experimentally accessible values, namely, the free and bound amounts of calcium and/or carbonate ions (n_{free} and n_{bound}, respectively) as well as the free calcium concentration (c_{free}). Corresponding fits provide evidence that the measured data are well described by the relation given in Eq. (3.9) and thus demonstrate that linear Ca^{2+} profiles are perfectly compatible with the model of multiple binding and the formation of associates larger than simple ion pairs. Evaluation of fitted data directly yields the number of binding sites for calcium on a carbonate ion (x) and the microscopic

equilibrium constant (K). These parameters can then be used to derive the actual calcium carbonate coordination within the clusters, N_{Calcium}, via (Demichelis et al., 2011)

$$N_{\mathrm{Calcium}} = x \cdot \frac{n_{\mathrm{bound}}(\mathrm{Ca}^{2+}) + n_{\mathrm{free}}(\mathrm{Ca}^{2+})}{n_{\mathrm{bound}}(\mathrm{Ca}^{2+})} \tag{3.10}$$

as well as their macroscopic thermodynamic stability (ΔG) according to (Gebauer et al., 2008)

$$\Delta G = \quad RT\ln(x \cdot K) \tag{3.11}$$

In the same way as the treatment according to Eq. (3.5) cannot fundamentally exclude that association may proceed beyond the ion pair, successful data analysis on the basis of multiple binding equilibria does not prove the existence of prenucleation clusters as such, either. However, we can now turn to discuss the explanatory power of this model. First, it may be regarded as the simplest approach to theoretically describe the formation of large (≥ 1 nm) ion associates in solution, which have been detected by means of AUC (see succeeding text) and cryo TEM (Kellermeier et al., 2012; Pouget et al., 2009), while still being in agreement with experimentally observed ion binding profiles. Second, the thermodynamic parameters resulting from the model indicate that the stability of the associated species varies with the pH of the system (Gebauer et al., 2008), which is hard to explain when admitting ion pairs only. In turn, changes in the internal structure of larger clusters may well account for these variations in stability. Furthermore, when considering that nucleation might occur through cluster–cluster aggregation (Kellermeier et al., 2012; Pouget et al., 2009), the model can rationalize why a more stable form of ACC is initially precipitated at lower than at higher pH values (Cartwright, Checa, Gale, Gebauer, & Sainz Díaz, 2012; Gebauer & Cölfen, 2011; Gebauer et al., 2010). This indicates that the clusters exhibit some kind of encoded proto structure that is conveyed into the emerging solid phase during nucleation. Last but not least, multiple binding analyses suggest that, on average, two calcium ions are bound per carbonate, and vice versa, throughout the entire cluster (Demichelis et al., 2011). This mean calcium carbonate coordination number hints at linear chains or rings of polymerized ion pairs (i.e., $\cdots \mathrm{Ca}^{2+} \quad \mathrm{CO_3}^{2} \quad \mathrm{Ca}^{2+} \quad \mathrm{CO_3}^{2} \cdots$, rather than $[\mathrm{CaCO_3}]^{0}$) and is consistent with dynamic structures observed in computer simulations of aqueous $\mathrm{CaCO_3}$ solutions (Demichelis et al., 2011). These so called

dynamically ordered liquid like oxyanion polymers (DOLLOPs) were proposed to represent the actual structural form of $CaCO_3$ prenucleation clusters.

4.3. Cluster detection and characterization in AUC

Figure 3.3 illustrates the principal setup of the sedimentation velocity experiments used to trace ion clusters in prenucleation $CaCO_3$ solutions. The analytical ultracentrifuge operates at very high rotational speeds that generate centrifugal accelerations in the range of $\sim 280{,}000 \times g$ ($\omega^2 r$, where ω is the

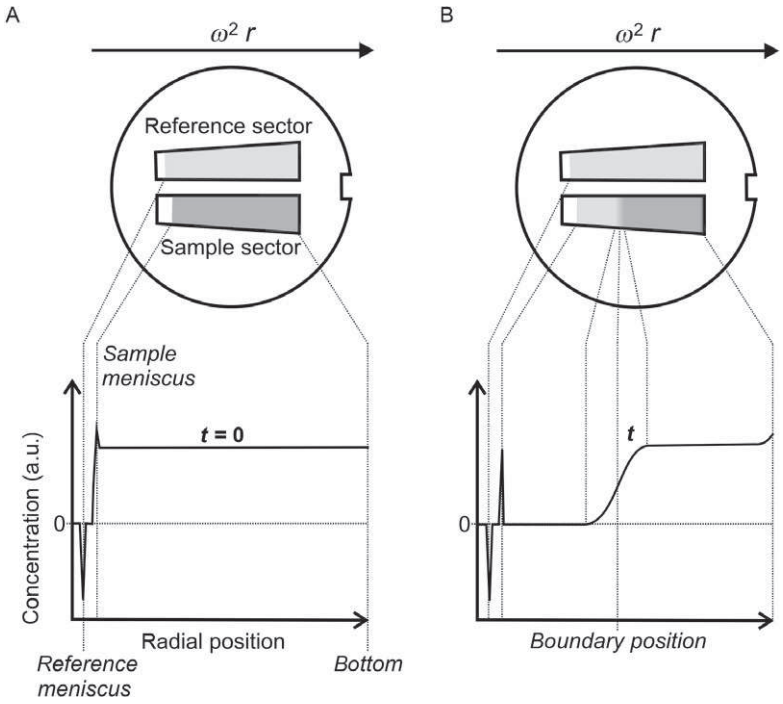

Figure 3.3 Principle of sedimentation velocity experiments in analytical ultracentrifugation. Sample and reference solutions are filled into sector-shaped titanium centerpieces (top) and then become exposed to a centrifugal field $\omega^2 r$ (ω, angular velocity; r, radial position). (A) Before the beginning of the experiment ($t = 0$), the solution to be analyzed is homogeneously distributed in the sample cell, and corresponding concentration profiles (bottom) indicate the position of the sample and reference meniscuses as sharp peaks (which are artifacts induced by the air/liquid interface). (B) After a certain time t, species present in the sample have sedimented to a certain degree, and the position of the sedimenting boundary can be determined from the measured concentration profile (bottom). Diffusion of the sedimenting species leads to progressive broadening of the boundary with time, as indicated.

angular velocity and r the distance from the center of rotation). The measurement cells are sector shaped (so as to avoid convection caused by collisions of sedimenting species with the wall of the cells) and aligned in the path of analytical optics, which allow for the determination of concentration profiles in the sample cell relative to a reference, typically water (Fig. 3.3A and B, top). Generally, different methods can be employed for monitoring the concentrations of species and their spatiotemporal development, such as UV–vis spectroscopy or interferometry. In case of the nonlight absorbing sedimenting ions and ion associates discussed here, the only detectable difference with respect to the solvent is the refractive index (n) and corresponding increments, which can be detected by means of a Rayleigh interferometer.

At the beginning of the experiment ($t=0$), the solution to be analyzed is continuously distributed in the sample cell, and the optics merely detect the meniscus of both sample and reference (Fig. 3.3A). After a certain time t, the solutes (or particles) of interest have sedimented due to the applied centrifugal field (Fig. 3.3B). By tracking the position of the sedimenting boundary as a function of time (i.e., experiment duration), the sedimentation velocity (v) can be obtained and used to derive the sedimentation coefficient ($s=v\omega^{-2}r^{-1}$), which is typically given in units of Svedberg ($1\ \mathrm{S}=10^{-13}$ s). In practice, data analyses are performed with the SEDFIT software (Schuck, 2000, 2013), where the measured time dependent sedimentation profiles are evaluated on the basis of the Lamm equation, which describes transport processes occurring due to concurrent sedimentation and diffusion in the experiments (note that diffusion leads to a broadening of the sedimenting boundary, which becomes more and more pronounced with time, cf. Fig. 3.3B).

Because the sedimentation of single ions is very slow and close to the detection limit of the technique, the uncertainty of corresponding s values is rather high (estimated to ca. 0.3 S) (Gebauer et al., 2008). Moreover, it is crucial to realize that there is a large excess of spectator ions in the buffer (in particular Na^+ and HCO_3^-, as well as the chloride ions introduced with Ca^{2+} during titration), which do not participate in cluster formation. In fact, calcium only makes up a fraction of about 1% of all present ions in typical samples (Gebauer et al., 2008). Depending on the pH, 30–70% of these calcium ions are bound in the prenucleation stage so that, compared to all free ions, the concentration of clusters is certainly low. To address this issue, the SEDFIT evaluation routines have been tested by simulations concerning whether they can give correct sedimentation coefficients for this

extreme situation; it was found that the applied procedure can distinguish a fraction of 1 wt% clusters next to an excess of 99% spectator ions (Gebauer et al., 2008), which thus is sufficient to characterize ion association in the studied systems.

Conventionally, AUC data are fitted to the Lamm equation utilizing a model that assumes noninteracting and monodisperse species and yields sedimentation as well as diffusion coefficients for a preset number of components (≤ 4). Each data set is evaluated for one, two, three, and four different species. Then, the best fit is chosen based on the quality of the SEDFIT parameters. When AUC analyses are carried out with samples drawn from the $CaCO_3$ crystallization assay before nucleation, clusters with $s = 1.4 \pm 0.8$ S are found with good statistical significance next to a majority of sedimenting ions ($s = 0.11 \pm 0.05$ S) (Gebauer et al., 2008). The clusters are reliably detected about as soon as the solution becomes supersaturated with respect to the initially precipitated phase, whereas their concentration seems to be too low in the undersaturated regime (we note, however, that ion association occurs in the same manner also below the saturation limit, where the presence of clusters has been confirmed by cryo TEM (Pouget et al., 2009)). A second, larger cluster species ($s = 5 \pm 1$ S) is observed close to the point of nucleation (yet with lower statistical relevance), while a third and even bigger population ($s \approx 7$–10 S) could occasionally be traced in solutions after nucleation (Gebauer et al., 2008).

In addition to the sedimentation coefficients, the SEDFIT routine also yields corresponding diffusion coefficients (D) for each of the distinct species, which can be derived from the broadening of the sedimenting boundary and converted into hydrodynamic diameters (d_H) utilizing the Stokes–Einstein equation:

$$d_H = \frac{k_B T}{3\pi\eta D} \tag{3.12}$$

where k_B is the Boltzmann constant, T the absolute temperature, and η the solvent viscosity. Since the sedimenting species are very small, sizes estimated on the basis of the diffusion coefficient should be more reliable than values obtained from sedimentation coefficients. However, while the free ions can be considered monodisperse within experimental accuracy, the clusters may well be polydisperse and, if so, the derived diffusion coefficients would be too high, because broadening of the boundary is in this case not caused by diffusion alone, but contains unknown contributions from the polydispersity of the analyzed species (i.e., its s distribution). In this regard,

diffusion coefficients determined for the clusters by Lamm modeling have to be regarded as upper limits, whereas diameters calculated from D via the Stokes–Einstein relation consequently represent lower limits (cf. Eq. 3.12). For the smallest cluster species (i.e., those reliably detected in supersaturated solutions with $s = 1.4$ S), Eq. (3.12) yields a diameter of 0.9 ± 0.2 nm, while 1.8 ± 0.5 and ~ 4 nm are calculated for the larger clusters observed close to and after nucleation, respectively (Gebauer et al., 2008).

Alternatively, the hydrodynamic diameter can also be directly obtained from the measured sedimentation coefficient by assuming spherically shaped clusters and applying the following equation:

$$d_H = \sqrt{\frac{18\eta s}{\rho_{Cluster} \quad \rho_S}} \tag{3.13}$$

where $\rho_{Cluster}$ and ρ_S are the densities of the clusters and the solvent, respec tively. Here, the major problem is that the density of the clusters is not known; in a first approximation, one may use the value of ACC ($\rho_{ACC} = 1.48$ g/mL (Cölfen & Völkel, 2006)), which is supposed to be the phase that nucleates through aggregation of the clusters. This gives sizes of 2.1 ± 0.6, 3.9 ± 0.4, and ca. 5 nm for the different cluster species dis cussed earlier (Gebauer et al., 2008). If the density of the clusters is lower than that of ACC (which is well possible as the solute clusters are expected to be more hydrated than nucleated ACC particles), corresponding diame ters become larger (cf. Eq. 3.13). Thus, s based cluster sizes must also be considered as lower limits.

Knowledge of the cluster size and density furthermore allows for an esti mation of the number of calcium and carbonate ions combined in single clusters (Gebauer et al., 2008). For example, a spherical cluster of 2 nm in diameter and with the density of ACC would contain about 35 formula units of calcium carbonate. Even though this may be a rough approximation, it is evident that the species detected next to single ions by means of AUC must be significantly larger, on average, than simple ion pairs. In our opinion, a realistic estimate is that typical clusters comprise some tens of ions, plus an as yet unknown amount of hydration water.

While the earlier considerations essentially reflect the AUC evaluation made for $CaCO_3$ clusters in the original work (Gebauer et al., 2008), we can now turn to discuss the results in light of recent insight gained by com puter simulations (Demichelis et al., 2011), which suggest that prenucleation

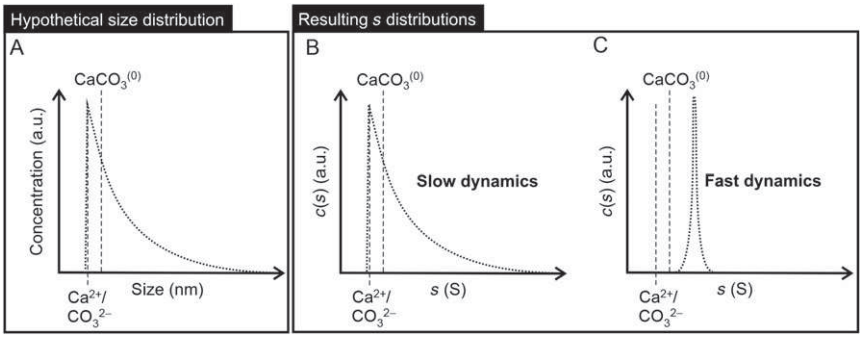

Figure 3.4 Hypothetical distributions for the size (A) and the diffusion-corrected sedimentation coefficient (B, C) of prenucleation clusters in case of slow (B) and fast dynamics (C) with respect to the duration of the experiment. In solution at room temperature, the dynamics of ion association are expected to be orders of magnitude faster than the typical duration of an AUC measurement (thus excluding scenario B). Therefore, AUC data reflect an average response and, depending on the chosen model, the mean values found for *s* will be significantly larger than those of single ions (C, model of prenucleation clusters). Note that spectator ions are neglected in the scheme and that peak integrals are not to scale.

clusters are in fact highly dynamic, chain like polymers of alternating Ca^{2+} and CO_3^{2} ions (DOLLOPs). In general, the size distribution expected for such dynamic polymers is rather broad (Fig. 3.4A), perhaps in analogy to the outcome of classical polycondensation reactions (Flory, 1936). In contrast to that, diffusion corrected sedimentation coefficient distributions obtained by AUC are very narrow, thus pointing toward fairly monodisperse species at first glance (Fig. 3.4C) (Gebauer et al., 2008). However, it must be taken into account that structural rearrangements of DOLLOPs occur on timescales of molecular processes in solution, that is, within hundreds of picoseconds (Demichelis et al., 2011), and that the clusters decompose and reform at rates that are multiple orders of magnitude faster than the duration of a typical AUC experiment (which takes several hours). Hence, it is impossible to resolve the polydispersity of these species in AUC (as hypothetically done in Fig. 3.4B), owing to their dynamics, and the values measured for *s* and *D* therefore reflect average states. In this regard, the apparent narrow size distribution indicated by AUC is perfectly consistent with the speciation envisaged in the DOLLOP concept, which has been proposed to explain the structure of $CaCO_3$ prenucleation clusters. Moreover, since the species involved in the formation of DOLLOPs (i.e., single Ca^{2+} and CO_3^{2}, ion pairs, and dimers of ion pairs) are all connected

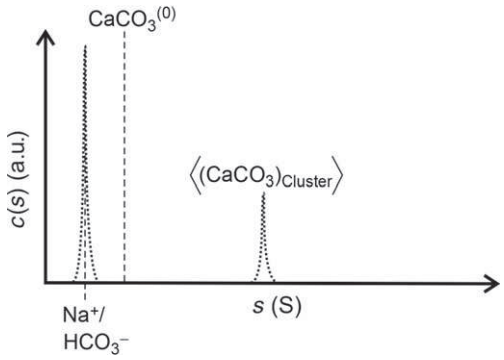

Figure 3.5 Schematic representation of typical *s*-distributions determined experimentally by means of AUC (integrals not to scale). The peak at low *s* originates from spectator ions in the buffer (primarily sodium and bicarbonate but also chloride ions), whereas the signal at higher *s* reflects the average of all associated calcium carbonate species that are interconnected by fast equilibria (i.e., the mean cluster size, as indicated by angle brackets).

by very fast equilibria, the mean size seen by AUC will be an average of all these states, weighted according to their relative abundance in the system. In other words, if there were only single ions and ion pairs, sedimentation and diffusion coefficients would reflect the average of these species and, hence, the determined sizes and *s* values would lie in between those of single ions and ion pairs. As this is not the case and the resulting hydrodynamic diam eters are distinctly larger (i.e., a scenario as depicted in Fig. 3.5), we conclude that ion association in aqueous $CaCO_3$ solutions proceeds beyond the ion pair, leading to the formation of prenucleation clusters. It further becomes clear that the actual population of single ions detected in the AUC exper iments comprises only the spectator ions mentioned earlier (Na^+ and HCO_3 in first place) and not Ca^{2+} and CO_3^{2} ions, which participate in the DOLLOP equilibria. The fact that larger clusters can be detected next to smaller clusters close to nucleation may indicate that the latter show dif ferent dynamics and are not connected to the smaller DOLLOPs by fast equilibria. This notion is also supported by computer simulations, which evidence a distinct change of DOLLOP dynamics above a certain critical size (Cartwright et al., 2012).

5. CONCLUSIONS AND OUTLOOK

We have described a crystallization assay that provides a straightfor ward means to assess ion association before, during, and after the nucleation of minerals in a quantitative manner. It further allows for the identification

of different precursor and intermediate stages, both in the absence and pres ence of additives, and thus renders them analytically accessible. Though not explicitly addressed here, the collected data can also be directly used to char acterize precipitation kinetics and, when studies are carried out at distinct temperatures, permit even deeper insights into the thermodynamics of ion binding and nucleation as such. By combining the crystallization assay with a high resolution technique like AUC, ion associates existing in solu tion prior to nucleation can be investigated in detail. For calcium carbonate, this methodology shows that ions assemble into clusters that are significantly larger than ion pairs, while size distributions obtained from the AUC mea surements agree with the dynamic structural form (DOLLOP) suggested for these prenucleation clusters on the basis of computer simulations. AUC is an absolute technique that, in our opinion, will turn out to be valuable also for analyses of interactions between crystallization additives and prenucleation species.

Experiments as those discussed in this work are crucial to gain a more profound understanding of the early stages of mineral precipitation, which is urgently needed and will have fundamental implications for diverse appli cations across various fields of research. Quantitative crystallization assays may contribute to achieve this by tracing distinct phases and intermediates on the way to final stable phases, which then can be studied by a range of analytical techniques including not only those introduced here but also others such as light scattering or *in situ* IR and Raman spectroscopy.

REFERENCES

Addadi, L., Raz, S., & Weiner, S. (2003). Taking advantage of disorder: Amorphous calcium carbonate and its roles in biomineralization. *Advanced Materials*, *15*, 959 970.

Banfield, J. F., Welch, S. A., Zhang, H. Z., Ebert, T. T., & Penn, R. L. (2000). Aggregation based crystal growth and microstructure development in natural iron oxyhydroxide biomineralization products. *Science*, *289*, 751 754.

Bewernitz, M. A., Gebauer, D., Long, J. R., Colfen, H., & Gower, L. B. (2012). A meta stable liquid precursor phase of calcium carbonate and its interactions with polyaspartate. *Faraday Discussions*, *159*, 291 312.

Cartwright, J. H. E., Checa, A. G., Gale, J. D., Gebauer, D., & Sainz Díaz, C. I. (2012). Cal cium carbonate polyamorphism and its role in biomineralization: How many amorphous calcium carbonates are there? *Angewandte Chemie, International Edition*, *51*, 11960 11970.

Colfen, H., & Antonietti, M. (2008). *Mesocrystals and nonclassical crystallization*. Chichester: John Wiley & Sons, Ltd.

Colfen, H., & Volkel, A. (2006). Application of the density variation method on calcium carbonate nanoparticles. *Progress in Colloid and Polymer Science*, *131*, 126 128.

Davey, R. J., Schroeder, S. L. M., & ter Horst, J. H. (2013). Nucleation of organic crystals A molecular perspective. *Angewandte Chemie, International Edition*, *52*, 2166 2179.

Demeler, B. (2005). UltraScan A comprehensive data analysis package for analytical ultra centrifugation experiments. In *Modern analytical ultracentrifugation: Techniques and methods* (pp. 210 229). Cambridge, UK: The Royal Society of Chemistry.

Demichelis, R., Raiteri, P., Gale, J. D., Quigley, D., & Gebauer, D. (2011). Stable prenucleation mineral clusters are liquid like ionic polymers. *Nature Communications*, *2*, 590.

Dey, A., de With, G., & Sommerdijk, N. A. J. M. (2010). In situ techniques in biomimetic mineralization studies of calcium carbonate. *Chemical Society Reviews*, *39*, 397.

De Yoreo, J. J., & Vekilov, P. G. (2003). Principles of crystal nucleation and growth. *Reviews in Mineralogy and Geochemistry*, *54*, 57 93.

Flory, P. J. (1936). Molecular size distribution in linear condensation polymers. *Journal of the American Chemical Society*, *58*, 1877 1885.

Fratzl, P., & Weiner, S. (2010). Bio inspired materials Mining the old literature for new ideas. *Advanced Materials*, *22*, 4547 4550.

Gal, J. Y., Bollinger, J. C., Tolosa, H., & Gache, N. (1996). Calcium carbonate solubility: A reappraisal of scale formation and inhibition. *Talanta*, *43*, 1497 1509.

Gebauer, D., & Colfen, H. (2011). Prenucleation clusters and non classical nucleation. *Nano Today*, *6*, 564 584.

Gebauer, D., Colfen, H., Verch, A., & Antonietti, M. (2009). The multiple roles of additives in $CaCO_3$ crystallization: A quantitative case study. *Advanced Materials*, *21*, 435 439.

Gebauer, D., Gunawidjaja, P. N., Ko, J. Y. P., Bacsik, Z., Aziz, B., Liu, L. J., et al. (2010). Proto calcite and proto vaterite in amorphous calcium carbonates. *Angewandte Chemie, International Edition*, *49*, 8889 8891.

Gebauer, D., Verch, A., Borner, H. G., & Colfen, H. (2009). Influence of selected artificial peptides on calcium carbonate precipitation A quantitative study. *Crystal Growth & Design*, *9*, 2398 2403.

Gebauer, D., Volkel, A., & Colfen, H. (2008). Stable prenucleation calcium carbonate clus ters. *Science*, *322*, 1819 1822.

Gower, L. B. (2008). Biomimetic model systems for investigating the amorphous precursor pathway and its role in biomineralization. *Chemical Reviews*, *108*, 4551 4627.

Izmailov, A. F., Myerson, A. S., & Arnold, S. (1999). A statistical understanding of nucle ation. *Journal of Crystal Growth*, *196*, 234 242.

Kellermeier, M., Gebauer, D., Melero García, E., Drechsler, M., Talmon, Y., Kienle, L., et al. (2012). Colloidal stabilization of calcium carbonate prenucleation clusters with silica. *Advanced Functional Materials*, *22*, 4301 4311.

Kellermeier, M., Picker, A., Kempter, A., Colfen, H., & Gebauer, D. (2013). A straightforward treatment of activity in aqueous $CaCO_3$ and its consequences for nucleation theory (submitted for publication).

Li, D., Nielsen, M. H., Lee, J. R. I., Frandsen, C., Banfield, J. F., & De Yoreo, J. J. (2012). Direction specific interactions control crystal growth by oriented attachment. *Science*, *336*, 1014 1018.

Lowenstam, H., & Weiner, S. (1989). *On biomineralization*. New York: Oxford University Press.

Machtle, W., & Borger, L. (2006). *Analytical ultracentrifugation of polymers and nanoparticles*. Berlin/New York: Springer.

Meldrum, F. C., & Colfen, H. (2008). Controlling mineral morphologies and structures in biological and synthetic systems. *Chemical Reviews*, *108*, 4332 4432.

Moore, E. W., & Verine, H. J. (1981). Pancreatic calcification: Formation constants of $CaHCO_3^+$ and $CaC0_3^{(0)}$ complexes determined with Ca^{2+} electrode. *American Journal of Physiology Gastrointestinal and Liver Physiology*, *241*, G182 G190.

Mullin, J. (2001). *Crystallization* (4th ed.). Oxford: Butterworth Heinemann.

Picker, A., Kellermeier, M., Seto, J., Gebauer, D., & Colfen, H. (2012). The multiple effects of amino acids on the early stages of calcium carbonate crystallization. *Zeitschrift für Kristallographie Crystalline Materials*, *227*, 744 757.

Planken, K. L., & Colfen, H. (2010). Analytical ultracentrifugation of colloids. *Nanoscale*, *2*, 1849 1869.
Pouget, E. M., Bomans, P. H. H., Goos, J. A. C. M., Frederik, P. M., de With, G., & Sommerdijk, N. A. J. M. (2009). The initial stages of template controlled $CaCO_3$ for mation revealed by cryo TEM. *Science*, *323*, 1455 1458.
Raiteri, P., & Gale, J. D. (2010). Water is the key to nonclassical nucleation of amorphous calcium carbonate. *Journal of the American Chemical Society*, *132*, 17623 17634.
Ralston, G. (1993). *Introduction to analytical ultracentrifugation*. Fullerton, CA: Beckman Instruments.
Robinson, R. A., & Stokes, R. H. (2002). *Electrolyte solutions* (2nd rev. ed.). Mineola, NY: Dover Publications.
Scatchard, G. (1949). The attractions of proteins for small molecules and ions. *Annals of the New York Academy of Sciences*, *51*, 660 672.
Schuck, P. (2000). Size distribution analysis of macromolecules by sedimentation velocity ultracentrifugation and Lamm equation modeling. *Biophysical Journal*, *78*, 1606 1619.
Schuck, P. (2013). *SEDFIT*. http://www.analyticalultracentrifugation.com.
Sommerdijk, N. A. J. M., & Colfen, H. (2010). Lessons from nature Biomimetic approaches to minerals with complex structures. *MRS Bulletin*, *35*, 116 121.
Tomson, M. B., & Nancollas, G. H. (1978). Mineralization kinetics: A constant composition approach. *Science*, *200*, 1059 1060.
Verch, A., Gebauer, D., Antonietti, M., & Colfen, H. (2011). How to control the scaling of $CaCO_3$: A "fingerprinting technique" to classify additives. *Physical Chemistry Chemical Physics*, *13*, 16811 16820.
Weiner, S., & Addadi, L. (2011). Crystallization pathways in biomineralization. *Annual Review of Materials Research*, *41*, 21 40.
Weiner, S., Mahamid, J., Politi, Y., Ma, Y., & Addadi, L. (2009). Overview of the amor phous precursor phase strategy in biomineralization. *Frontiers of Materials Science in China*, *3*, 104 108.